Chinese Chemical Letters 37 (2026) 111613

Contents lists available at ScienceDirect

Chinese Chemical Letters

journal homepage: www.elsevier.com/locate/cclet

Cocrystal engineering for constructing emissive ambipolar semiconductor based on diphenylanthracene and diperfluorophenylanthracene

Liangliang Chen[a,*], Han Huang[d], Qingqiu Zhu[a], Yiyun Zeng[a], Zhichun Shangguan[b,*], Jin Chen[a], Xunchang Wang[a,*], Cheng Li[c], Guanxin Zhang[c], Hongbing Fu[d], Deqing Zhang[c]

[a] Key Laboratory of Flexible Optoelectronic Materials and Technology (Ministry of Education), School of Optoelectronic Materials & Technology, Jianghan University, Wuhan 430056, China
[b] College of Chemistry and Materials Engineering, Wenzhou University, Key Lab of Biohealth Materials and Chemistry of Wenzhou, Wenzhou 325027, China
[c] Beijing National Laboratory for Molecular Sciences, Institute of Chemistry, Chinese Academy of Sciences, Beijing 100190, China
[d] Beijing Key Laboratory for Optical Materials and Photonic Devices, Department of Chemistry, Capital Normal University, Beijing 100048, China

ARTICLE INFO

Article history:
Received 10 April 2025
Revised 14 July 2025
Accepted 18 July 2025
Available online 20 July 2025

Keywords:
Charge-transfer complex
Organic field-effect transistor
Ambipolar charge transport
Fluorescent emission

ABSTRACT

Organic ambipolar emitting materials hold immense potential for application in integrated optoelectrical devices yet challenging to design and synthesize. Cocrystals exhibit significant superiority in designing such materials because the properties of emission and transport can be flexibly tailored through the strategic pairing of donor and acceptor units. In this study, we report a new cocrystal system, DPA-5FDPA, derived from two high-mobility emissive molecules, 2,6-diphenylanthracene (DPA) and 2,6-diperfluorophenyl anthracene (5FDPA). This cocrystal system exhibits outstanding emission and ambipolar semiconducting properties. Notably, the single-crystal field-effect transistor devices based on DPA-5FDPA achieve maximum hole and electron mobilities of 0.298 cm^2 V^{-1} s^{-1} and 0.009 cm^2 V^{-1} s^{-1}, respectively. In comparison, the reference compound of 2-perfluorophenyl-6-phenylanthracene (5FBA) exhibits unipolar p-type transport with the hole mobility of 0.008 cm^2 V^{-1} s^{-1}. In addition, DPA-5FDPA exhibits excellent optical waveguide behavior with a small optical loss coefficient of 0.079 dB/μm at 508 nm, which is lower than most reported cocrystal systems. These results underscore the promise of co-crystallization as a versatile strategy for developing advanced ambipolar emissive semiconductors and provide deeper insights into the relationships among molecular structures, packing modes, intermolecular interactions, and charge-transport properties.

© 2025 Published by Elsevier B.V. on behalf of Chinese Chemical Society and Institute of Materia Medica, Chinese Academy of Medical Sciences.

Organic emissive semiconducting materials integrating luminescent and carrier-transporting properties have garnered significant attention for their potential applications in multifunctional optoelectronic devices and integrated circuit fabrication, particularly for ambipolar emissive semiconductors [1–5]. So far, the majority of the reported organic optoelectrical materials only exhibit unipolar transporting behaviors mainly due to the unbalanced electronic coupling of the frontier molecular orbitals (FMO) [6,7], and only a few are ambipolar [8–10]. Several strategies have been explored to achieve ambipolar transport, such as donor (D)/acceptor (A) blends or bilayers [11–13]. However, these systems suffer from low carrier mobility and fluorescence quenching because of the phase separation or mismatched FMO energy levels, which restricts their practical applicability in high-performance optoelectronic devices [14,15].

Co-crystallization of the appropriate D and A molecules to form a charge-transfer (CT) D-A complex has been demonstrated as a valid approach to improve various functions, including luminescence [16–21], and ferroelectricity and multiferroics [22–24], optical waveguiding [25–27], nonlinear optical [28,29] and stimuli-responsiveness [30,31] as well as ambipolar charge transport [32–35]. Generally, cocrystals not only retain the intrinsic physical and chemical features of individual components, but may also show new properties induced by the cooperative effect of individual constituents through noncovalent intermolecular interaction [36,37], such as CT interaction, hydrogen bond, halogen bond, and π-π interaction [38–48]. Consequently, co-crystallization has been considered to be a promising way to design and synthesize am-

* Corresponding authors.
E-mail addresses: chenliangliang@jhun.edu.cn (L. Chen), sgzc@live.cn (Z. Shangguan), wangxc@jhun.edu.cn (X. Wang).

https://doi.org/10.1016/j.cclet.2025.111613
1001-8417/© 2025 Published by Elsevier B.V. on behalf of Chinese Chemical Society and Institute of Materia Medica, Chinese Academy of Medical Sciences.

bipolar semiconducting materials with strongly emissive properties [49,50]. However, most reported cocrystal materials with ambipolar transport exhibit weak or even negligible emission, which is attributed to the strong CT interaction between D and A units. For example, TTF-TCNQ-based cocrystals are typical ambipolar CT complexes, but these cocrystals are non-emissive [12,51,52]. Similarly, Hu *et al*. reported a series of cocrystal systems with TCNQ or perylene diimide as acceptors and polycyclic aromatic hydrocarbons (fluorene, anthracene, pyrene and perylene, *etc*.) as donors. These systems exhibit ambipolar or n-type charge transport behavior, but they are poorly emissive with extremely low photoluminescent quantum yield (PLQY) [32,53,54]. On the other hand, co-crystallization of aromatic fluorophores with molecular barrier can reduce aggregation-caused quenching (ACQ) effect, thus greatly enhancing the PLQY [21]. For example, Zhang *et al*. selected octafluoronaphthalene (OFN) as a molecular barrier to impede intermolecular interaction and electron exchange among fluorophores (anthracene, perylene or coronene), which blocks the single-triplet pathway, resulting in nearly 100% PLQY [20]. Yet, cocrystals that integrate fluorescence and ambipolar charge-transport properties are rarely reported. In 2013, Park *et al*. first reported a D-A cocrystal system containing distyrylbenzene (4M-DSB)- and dicyanodistyrylbenzene (CN-TFPA)-based molecules, which shows an efficient red emission with PLQY of 31% and ambipolar transport with hole mobility (μ_h) and electron mobility (μ_e) of 6.7×10^{-3} cm^2 V^{-1} s^{-1} and 6.7×10^{-2} cm^2 V^{-1} s^{-1} [55], respectively. Subsequently, they selected dicyanodistyrylbenzene (2MDSC) as the donor and CN-TFPA as the acceptor to form a new cocrystal (CT3), achieving a higher PLQY of 60% and balanced ambipolar transport (μ_h and μ_e of *ca.* 10^{-4} cm^2 V^{-1} s^{-1}). Besides, CT3-based organic light-emitting transistor (OLET) devices exhibited external quantum efficiency (EQE) up to 1.5% [56]. However, the carrier mobilities of these cocrystal systems are far lower than their individual components and the advantages of cocrystals for optoelectronic materials have not been fully demonstrated in other cocrystal systems.

Herein, we report a new cocrystal system (DPA-5FDPA), based on 2,6-diphenylanthracene (DPA) and 2,6-diperfluorophenyl anthracene (5FDPA), as an emissive ambipolar semiconductor. The rationale behind the molecular design is as follows: (i) DPA has been established as a high-mobility emissive semiconductor, with a PLQY of 41.2% and a μ_h of 34 cm^2 V^{-1} s^{-1} [57], making it a promising donor constituent for cocrystal. Similarly, 5FDPA exhibits n-channel charge transport behavior with an impressive μ_e of 2.65 cm^2 V^{-1} s^{-1} and a PLQY of 52% [10], positioning it as an ideal acceptor component. (ii) The molecular sizes and packing modes of DPA and 5FDPA are highly compatible, owing to the similar atomic radius of hydrogen and fluorine. This structural similarity facilitates efficient packing and intermolecular interactions. (iii) Strong intermolecular hydrogen bonding occurs between the hydrogen atoms of DPA and the fluorine atoms of 5FDPA, enhancing the stability of the cocrystal. The cocrystal of DPA-5FDPA was successfully prepared *via* direct sublimation of a 1:1 mixture of DPA and 5FDPA. The resulting cocrystal exhibits a unique 1:1 mixed stacking pattern, which is conducive to ambipolar charge transport. Single-crystal field-effect transistors (FET) devices, which were fabricated with DPA-5FDPA cocrystal, demonstrated ambipolar charge transport properties, with the maximum μ_h of 0.298 cm^2 V^{-1} s^{-1} and μ_e of 0.009 cm^2 V^{-1} s^{-1}. Additionally, DPA-5FDPA displayed a red-shifted emission compared to its constituents of DPA and 5FDPA, with a PLQY of 16.8%. In comparison, 2-perfluorophenyl-6-phenylanthracene (5FBA), exhibited only p-channel charge transport property, highlighting the superiority of the cocrystal system in ambipolar transporting. These findings deepen our understanding of the interplay among molecular structures, intermolecular interactions, and charge transport properties. They also provide valuable guidance for designing more advanced ambipolar emissive cocrystal systems for organic optoelectronic applications.

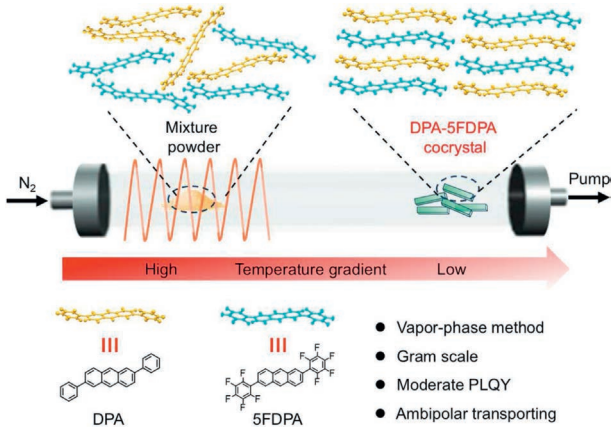


Fig. 1. The schematic diagram of the preparation of DPA-5FDPA cocrystal by vapor-phase method.

DPA and 5FDPA were synthesized according to the literature and subsequently purified *via* physical vapor transport (PVT), affording high-quality single crystals of both compounds [10,57]. As illustrated in Fig. 1, the cocrystal synthesis began with thoroughly mixing DPA and 5FDPA in a 1:1 molar ratio by grinding the powders for several minutes. The mixture was then placed in the high-temperature zone of the sublimation setup. Upon heating at 200 °C under a vacuum of 10^{-1} Pa, the green-emissive cocrystal of DPA-5FDPA was successfully deposited in the low-temperature zone. Compared to traditional solution evaporation or diffusion methods, the PVT method we employed offers significant advantages in the preparation of large quantities of cocrystalline materials [14,49]. Remarkably, the PVT approach used in this study enabled the production of the DPA-5FDPA cocrystal on a gram scale. This achievement is attributed to the highly similar chemical structures of DPA and 5FDPA, which facilitate efficient and scalable cocrystal formation, making this cocrystal system of DPA-5FDPA possible as a promising organic optoelectronic material. For comparison, the reference compound 5FBA was also prepared, with the detailed synthetic route provided in Supporting information. Thermogravimetric analysis (TGA) shows the onset decomposition temperature of DPA, 5FDPA, DPA-5FDPA and 5FBA are 276, 246, 262 and 241 °C, respectively (Fig. S1 in Supporting information), indicating these materials are stable enough upon heating at 200 °C.

The packing mode and intermolecular interactions of DPA, 5FDPA, DPA-5FDPA as well as the reference compound 5FBA were unveiled through single-crystal X-ray diffraction analysis. As shown in Fig. 2b, molecules of DPA and 5FDPA in the cocrystal exhibit twist configurations with the dihedrals between the anthracene and phenyl or perfluorophenyl groups of 41.34° and 48.24°, respectively. The dihedral angle between the anthracene and phenyl groups in DPA is found to be 19.97° (Fig. S2 in Supporting information), which is smaller than that observed in DPA-5FDPA. Conversely, the dihedral angle in 5FDPA was measured at 54.48° (Fig. S3 in Supporting information), larger than that in DPA-5FDPA. These findings suggest that the structural differences between DPA and 5FDPA are minimized through co-crystallization. To elucidate the convergency trend of the dihedral angles of the DPA and 5FDPA in the cocrystal, we first analyze the molecular packing and interaction of the cocrystal. Fig. 2a shows the packing mode and intermolecular interactions within the DPA-5FDPA cocrystal, which markedly differ from those of the individual DPA and 5FDPA crystals (Figs. S2 and S3). In the cocrystal, molecules of DPA and 5FDPA are alternatingly arranged to form molecular columns, in-

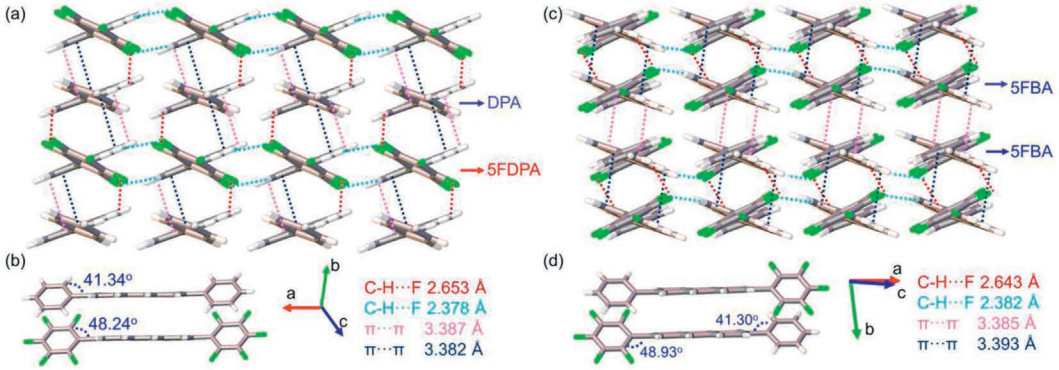


Fig. 2. The intermolecular interactions and packing modes of (a) DPA-5FDPA and (c) 5FBA. The dihedral angles between anthracene and phenyl or perfluorophenyl groups in (b) DPA-5FDPA and (d) 5FBA.

terconnected by C–H···F interactions with distances of 2.653 and 2.378 Å. Furthermore, intermolecular π–π stacking interactions are observed between the anthracene units of neighboring DPA and 5FDPA molecules, with distances of 3.387 and 3.382 Å, respectively. In contrast, the single crystals of DPA and 5FDPA adopt a herringbone packing mode without π–π interactions. The primary intermolecular interactions in DPA involve multiple C–H···π interactions with distances of 2.849, 2.873, and 2.860 Å, as shown in Fig. S2. Meanwhile, the 5FDPA crystal features multiple C–H···π (2.796 Å and 2.774 Å), C–F···π (3.090 Å), and C–H···F (2.596 and 2.572 Å) interactions (Fig. S3). The stronger intermolecular interaction in the cocrystal contributed to more tightly intermolecular packing, which is conducive to the convergence of dihedral angles of the individual components. To further illustrate this phenomenon, we conducted a relaxed potential energy scan to explore how the electronic energies of DPA and 5FDPA change as their dihedral angles vary from 0° to 90°. As shown in Fig. S4 (Supporting information), both molecules reach their minimum energy at dihedral angles near 40°, which is close to the conformations observed in the cocrystal (DPA: 41.33°, 5FDPA: 48.24°). These results indicate that increasing the dihedral angle of DPA while decreasing that of 5FDPA can effectively lower the energy of the cocrystal system. As shown in Fig. 2c, molecules of 5FBA in the crystal are arranged in a head-to-tail one-dimensional columnar packing manner. The dihedral angles between the anthracene and the substituted phenyl or perfluorophenyl groups are 41.30° and 48.93° (Fig. 2d), respectively, which is nearly identical to those observed in DPA-5FDPA (Figs. 2b and d). The main intermolecular interactions in 5FBA are also the same as DPA-5FDPA, including multiple C–H···F (2.643 and 2.382 Å) and π-π (3.385 and 3.393 Å) interactions (Fig. 2c). These results underscore the significant impact of D-A interactions on molecular packing and intermolecular interactions.

Powder X-ray diffraction (PXRD) measurements were performed to further confirm the structural consistency of the obtained cocrystal. As shown in Fig. 3a, the PXRD pattern of DPA-5FDPA displays strong and sharp diffraction peaks that are significantly different from those of the individual components, indicating that DPA-5FDPA is not a physical mixture of DPA and 5FDPA. Additionally, the PXRD patterns of DPA-5FDPA align well with the simulated diffraction data derived from the cocrystal, demonstrating that the DPA-5FDPA cocrystal powders are ultrapure and consist of a single crystalline phase.

As shown in Fig. 3b, the solid-state absorption spectrum of the cocrystal DPA-5FDPA exhibited a notable redshift in comparison with that of 5FDPA, but a slight blue-shift by comparing with that of DPA. 5FBA exhibited solid-state absorption spectra similar to those of DPA-5FDPA, indicating analogous electronic transition characteristics between the two crystalline systems, as will be discussed in detail below. Fig. 3c shows the emissive properties of DPA-5FDPA, DPA and 5FDPA. By comparing with DPA and 5FDPA, the emission spectrum of DPA-5FDPA was significantly red-shifted, while 5FBA displays an even further red shift. The DPA crystals with microplate shape exhibit cyan emission with a PLQY of 41 %, featuring distinct vibronic bands at 449, 476, 504 and 556 nm [57]. Similarly, the microplates of 5FDPA display emissions at 415, 436, 460, and 493 nm with a high PLQY of 52 % [10]. After co-crystallization, DPA-5FDPA forms microrod-shaped crystals exhibiting green emission, with the PLQY decreasing to 17 % (Fig. 3d). For 5FBA, its PLQY also decreased to 16 %. The red-shifted emission and the decrease in PLQY for DPA-5FDPA may be attributed to strong intermolecular charge transfer, while for 5FBA, it is caused by the combined effect of intermolecular and intramolecular charge transfer. Additionally, the average fluorescence lifetimes of DPA, 5FDPA, DPA-5FDPA as well as 5FBA were determined to be 4.83, 11.11, 23.95, 14.94 ns, respectively (Fig. S7 in Supporting information). Based on PLQY and lifetime results, DPA-5FDPA exhibits the smallest radiative rate of $7.01 \times 10^6\ s^{-1}$ in comparison with that of DPA ($8.49 \times 10^7\ s^{-1}$) and 5FDPA ($4.68 \times 10^7\ s^{-1}$) (Table S1 in Supporting information), further demonstrating strong charge transfer interactions between DPA and 5FDPA in the cocrystal.

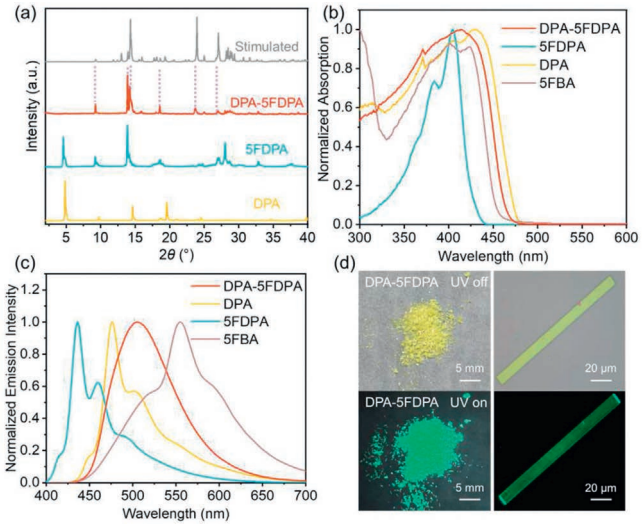


Fig. 3. (a) PXRD patterns of DPA, 5FDPA and DPA-5FDPA. The (b) solid-state absorption and (c) fluorescent emission spectra of DPA, 5FDPA, DPA-5FDPA and 5FBA. (d) Fluorescence microscope images of DPA-5FDPA.

Interestingly, DPA-5FDPA exhibits mechanical responsiveness. Upon grinding the green-emission cocrystal powder, which initially

has a *CIE* coordinate of (0.23, 0.50), the emission peak undergoes a substantial redshift to 538 nm, with a corresponding *CIE* coordinate change to (0.35, 0.52) (Fig. S8 in Supporting information). This fluorescence responsiveness is likely due to a transition from the crystalline to an amorphous state, as supported by the PXRD patterns shown in Fig. S19 (Supporting information). To exclude the effect of physical blend on the fluorescent responsive property, we have compared the fluorescent spectra of DPA-5FDPA cocrystal and the physical blend of DPA and 5FDPA with a molar ratio of 1:1. As shown in Fig. S10 (Supporting information), the emission spectrum of the blend is completely different from that of the ground cocrystal, demonstrating the mechanochromic response does not arise from simple physical mixing. In addition, the PXRD pattern of the mixture shows sharp diffraction peaks including the peaks of DPA and 5FDPA, as shown in Fig. S21 (Supporting information), suggesting the crystallinity of DPA and 5FDPA is less affected by physical blending. In contrast, the peak intensity of the cocrystal decreases significantly or even disappears after grinding, which further excludes the contribution of physical mixing to the mechanochromic responsive property.

Similarly, the individual component of DPA and 5FDPA also exhibits mechanical responsiveness. As shown in Fig. S11 (Supporting information), the crystalline DPA solid exhibits distinct vibronic bands at 449, 476, 504 and 556 nm. After grinding, the wavelength of the emission peaks showed almost no changes, while the relative intensity of the respective peaks changed a lot. The long-wavelength emission intensity increased and broadened as shown in Fig. S11a (Supporting information). The corresponding *CIE* coordinate of DPA changes from (0.332, 0.411) to (0.233, 0.407) as shown in Fig. S11b (Supporting information). 5FDPA also exhibits mechanical responsiveness, which has been investigated in detail in our previous work [10]. In contrast, 5FBA shows no distinct change before and after grinding, indicating this molecule exhibits no responsiveness to external forces.

The CT interactions and photophysical properties of cocrystals have been thoroughly elucidated through density functional theory (DFT) calculations. Fig. S16 (Supporting information) depicts that the cocrystal system of DPA-5FDPA displays a significant static dipole moment (SDM) of 1.049 D oriented from 5FDPA towards the DPA molecule, confirming the presence of CT interactions in the ground state. Non-covalent interaction (NCI) analysis and the calculated HOMO and LUMO distributions further support this conclusion. The NCI analysis shows a large green pattern between DPA and 5FDPA segments of the cocrystal system (Fig. S17 in Supporting information), suggesting the CT interactions exist in DPA-5FDPA. As shown in Fig. S18 (Supporting information), the HOMO and LUMO orbitals of respective molecules of DPA and 5FDPA are uniformly distributed on the anthracene skeletons, whereas the HOMO and LUMO orbitals of DPA-5FDPA are localized on DPA and 5FDPA units, respectively. In addition, the absorption spectrum, as well as corresponding electronic transitions of the cocrystal of DPA-5FDPA are also calculated based on TD-DFT calculations. Fig. 4a shows the two main absorption peaks of DPA-5FDPA. The long-wavelength absorption at 398.87 nm (3.1084 eV) is assigned to $S_0 \rightarrow S_3$ transition from HOMO-1 → LUMO excitation with the oscillator strength (*f*) of 0.1199 (Fig. 4c). Similarly, another observed absorption of 279.99 nm (3.80 eV) is attributed to the $S_0 \rightarrow S_{19}$ transition, which is mainly from the HOMO-1 → LUMO+2 and HOMO-2 → LUMO+1 excitations with a high *f* of 2.4166 (Fig. 4c). Notably, the band gap of DPA-5FDPA is calculated to be 3.18 eV, significantly smaller than the respective components, 3.45 eV for DPA and 3.46 eV for 5FDPA, illustrating the CT interaction between DPA and 5FDPA molecules (Fig. S18 in Supporting information). These results agree well with our experimental conclusion.

Furthermore, the photophysical properties and electronic transition process of 5FBA have also been calculated by TD-DFT as

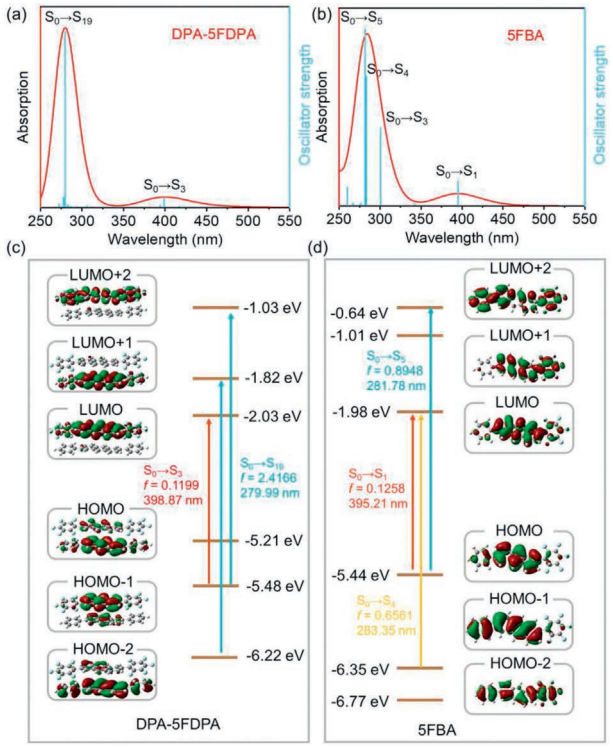


Fig. 4. The calculated absorption spectra of (a) DPA-5FDPA and (b) 5FBA. The corresponding electronic transitions of (c) DPA-5FDPA and (d) 5FBA.

shown in Fig. 4d. The HOMO orbital of 5FBA is mainly located at the phenyl group and anthracene unit, while LUMO is localized on the perfluorophenyl group and anthracene, indicating the intramolecular charge transfer exists in the 5FBA molecule. These intramolecular CT interactions also manifested in the red shift of the emission spectrum as discussed above. As shown in Figs. 4b and d, the absorption peak of 395.21 nm (3.1372 eV) is attributed to $S_0 \rightarrow S_1$ (HOMO → LUMO) transition with an oscillator strength of 0.1258. The continuous transition processes of $S_0 \rightarrow S_3$, $S_0 \rightarrow S_4$ and $S_0 \rightarrow S_5$ contribute significantly to the short-wavelength absorption peak of 285 nm. As a consequence, the calculated absorption is in accordance with the measured absorption spectrum as shown in Fig. 3b.

To investigate the charge-transport property of DPA-5FDPA, FET devices were fabricated based on the microrods of DPA-5FDPA and the device fabrication processes were provided in supporting information in detail. Unlike DPA, which exhibits p-channel transport, and 5FDPA, which shows n-channel transport, DPA-5FDPA demonstrates ambipolar semiconducting properties based on the transfer and output curves (Figs. 5a-d). The devices exhibited maximum μ_h and μ_e of 0.298 $cm^2\ V^{-1}\ s^{-1}$ and 0.009 $cm^2\ V^{-1}\ s^{-1}$, respectively (Table S5 in Supporting information). Analysis of X-ray diffraction (XRD) of cocrystal on the substrate and selective area electron diffraction (SAED) data (Figs. 5e and f) reveals that the charge-transporting direction in DPA-5FDPA aligns with the [100] crystallographic plane.

According to previous investigations [53,58], the hole transporting of the cocrystals is facilitated through super-exchange interactions of DPA molecules through molecules of 5FDPA, while the electron transporting is through super-exchange interactions of molecules of 5FDPA through molecules of DPA. This agrees well with the relatively large super-exchange integrals for the hole than electron transporting, which were calculated to be 103 and 35.7 meV, respectively (Fig. S23 in Supporting information).

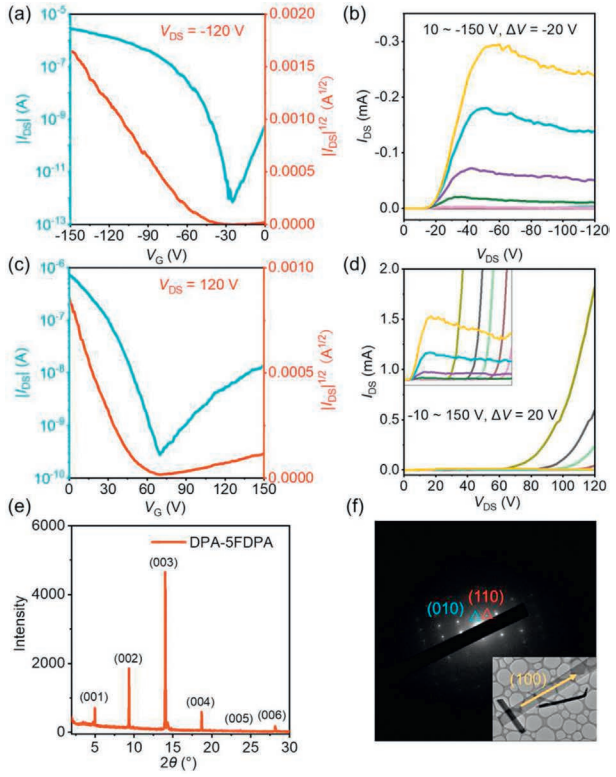


Fig. 5. The typical transfer curves of DPA-5FDPA for (a) p-channel and (c) n-channel operation modes. The typical output curves of DPA-5FDPA for (b) p-channel and (d) n-channel operation modes. (e) The XRD pattern of DPA-5FDPA. (f) The TEM image of DPA-5FDPA and its corresponding SAED pattern.

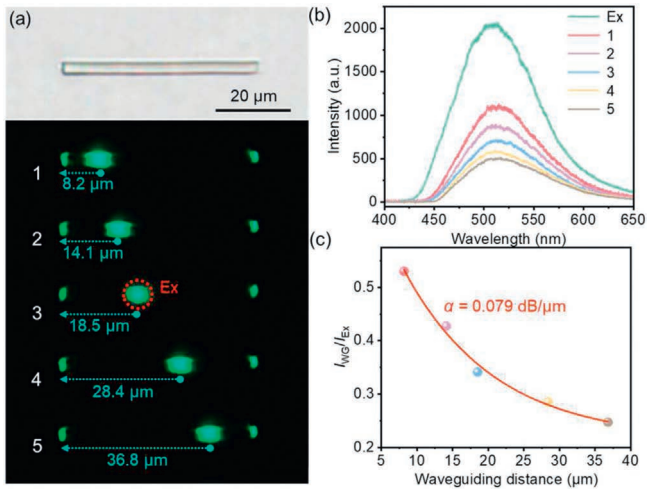


Fig. 6. (a) The photoluminescence images of the microrods of DPA-5FDPA. (b) The corresponding spatially resolved photoluminescence spectra of the out-coupled light at the end of the microrods of DPA-5FDPA. (c) Ratio of photoluminescence intensity at 508 nm of I_{WG}/I_{Ex}, against the propagation distance for microrods of DPA-5FDPA.

The semiconducting property of 5FBA was also investigated based on the film bottom-gate bottom-contact (BGTC) FET devices. Unlike DPA-5FDPA, which exhibits ambipolar transport, 5FBA exhibited unipolar p-channel transport with the hole mobility of 0.008 cm^2 V^{-1} s^{-1}, and no n-channel transport behavior was observed according to the transfer curve (Fig. S24 in Supporting information). The distinct transport behaviors between 5FBA and DPA-5FDPA may be due to the existing superexchange interaction in the cocrystal system despite the similar intermolecular packing and interactions for 5FBA and DPA-5FDPA. This suggests that the electronic properties and charge-transport mechanisms are strongly influenced by the specific molecular arrangements and interactions within cocrystals. These findings highlight the advantages of the cocrystal strategy in the design of ambipolar emissive semiconducting materials, offering a promising pathway to achieve tailored charge-transport and optical properties that are unattainable in single-component systems.

Moreover, we have noticed that bright green-luminescent spots were observed at the ends of microrod crystals of DPA-5FDPA as shown in Fig. 3d, while emissions in the middle of the cocrystal were relatively weak, indicating microrods of DPA-5FDPA exhibit typical optical waveguiding behavior. To further explore this phenomenon, the optical waveguiding properties within the microrods were investigated, and spatially resolved photoluminescence (PL) spectra were measured. Fig. 6b shows the microarea PL spectra recorded at the ends of the microrod under excitation with a 405 nm laser beam at different positions (labeled as 1, 2, 3, 4, and 5, Fig. 6a). The emission peak was located at 508 nm, which agrees well with the steady PL spectra, indicating that the self-absorption is minimal. When the laser was focused on the cocrystal, the emitted photons were confined within the microrod and propagated along the direction of crystal growth, identified as the [100] direction. In addition, the emission intensity collected from the tip of the cocrystal decreases continuously with the increase of propagation distance, while the emission intensities at the excitation points are almost the same along the microrods (Figs. 6a and b) This behavior was quantified through a single-exponential decay curve (Fig. 6c), which relates the intensity ratio of the incident (I_{Ex}) and outcoupled (I_{WG}) light to the propagation distance. This curve was fitted according to the function of $I_{WG}/I_{Ex} = Aexp(-RD)$, where A and D are constants [59,60]. Thus, the resulting optical loss coefficient for the microrod of DPA-5FDPA was calculated to be 0.079 dB/μm at 508 nm, which is one of the best optical waveguide performances in cocrystal systems according to our best knowledge (Table S2 in Supporting information). The exceptional optical waveguiding performance and low optical loss coefficient are attributed to the negligible self-absorption in DPA-5FDPA. This arises from the minimal overlap between the absorption and fluorescence spectra of DPA-5FDPA in the crystalline state (Fig. S9 in Supporting information), ensuring efficient light propagation with minimal energy loss.

In summary, we have successfully designed a new cocrystal system, DPA-5FDPA, derived from two structurally similar molecules, DPA and 5FDPA. Impressively, DPA-5FDPA exhibited 1:1 mixed stacking with an alternating arrangement to form molecular columns, distinctly different from the herringbone packing observed in the individual DPA and 5FDPA crystals. Besides, the fluorescent emission peak of DPA-5FDPA is red-shifted to 506 nm with a PLQY of 16.8 %, which is attributed to the intermolecular π-π and CT interactions between DPA and 5FDPA. This cocrystal shows ambipolar charge-transporting characteristics in the single-crystal FET devices, achieving maximum hole and electron mobilities of 0.298 cm^2 V^{-1} s^{-1} and 0.009 cm^2 V^{-1} s^{-1}, respectively. In contrast, the asymmetrically substituted compounds of 5FBA only show unipolar p-channel transport even though the packing modes and intermolecular interaction are the same with DPA-5FDPA, indicating the superexchange interaction in cocrystal of DPA-5FDPA plays an important role in ambipolar transport. Additionally, DPA-5FDPA demonstrates good optical waveguide behavior with a small optical loss coefficient of 0.079 dB/μm at 508 nm, which is one of the best-reported values for cocrystal systems. These results reveal that DPA-5FDPA is a promising ambipolar emissive organic material for integrated multifunctional optoelectrical devices. This study not only provides a new strategy for designing ambipolar emissive

materials, but also deepens our understanding of the relationship among molecular structures, packing modes, intermolecular interaction and charge transport properties.

Declaration of competing interest

The authors declare that they have no known competing financial interests or personal relationships that could have appeared to influence the work reported in this paper.

CRediT authorship contribution statement

Liangliang Chen: Writing – review & editing, Writing – original draft, Methodology, Investigation, Formal analysis, Data curation, Conceptualization. **Han Huang:** Methodology, Data curation. **Qingqiu Zhu:** Validation, Data curation. **Yiyun Zeng:** Validation, Methodology. **Zhichun Shangguan:** Writing – review & editing, Validation, Formal analysis, Data curation. **Jin Chen:** Validation, Methodology. **Xunchang Wang:** Writing – review & editing, Methodology, Funding acquisition. **Cheng Li:** Validation, Formal analysis. **Guanxin Zhang:** Validation, Methodology. **Hongbing Fu:** Validation, Methodology. **Deqing Zhang:** Writing – review & editing, Supervision, Funding acquisition.

Acknowledgment

This work was jointly supported by the National Natural Science Foundation of China (Nos. 22090021, 52203225).

Supplementary materials

Supplementary material associated with this article can be found, in the online version, at doi:10.1016/j.cclet.2025.111613.

References

[1] Z. Qin, H. Gao, H. Dong, W. Hu, Adv. Mater. 33 (2021) e2007149.
[2] C.F. Liu, X. Liu, W.Y. Lai, W. Huang, Adv. Mater. 30 (2018) e1802466.
[3] M.U. Chaudhry, K. Muhieddine, R. Wawrzinek, et al., Adv. Funct. Mater. 30 (2019) 1905282.
[4] D. Yuan, V. Sharapov, X. Liu, L. Yu, ACS Omega 5 (2020) 68–74.
[5] R. Capelli, S. Toffanin, G. Generali, et al., Nat. Mater. 9 (2010) 496–503.
[6] Y. Sakamoto, T. Suzuki, M. Kobayashi, et al., J. Am. Chem. Soc. 126 (2004) 8138–8140.
[7] L. Chen, Y. Wang, Z. Liu, Asian J. Org. Chem. 14 (2024) e202400608.
[8] Y. Zhang, Y. Wang, C. Gao, et al., Chem. Soc. Rev. 52 (2023) 1331–1381.
[9] Q. Li, Y. Zhang, J. Lin, et al., Angew. Chem. Int. Ed. 62 (2023) e202308146.
[10] L. Chen, Z. Qin, H. Huang, et al., Adv. Sci. 10 (2023) e2300530.
[11] A. Gumyusenge, D.T. Tran, X. Luo, et al., Science 362 (2018) 1131–1134.
[12] H. Alves, A.S. Molinari, H. Xie, A.F. Morpurgo, Nat. Mater. 7 (2008) 574–580.
[13] A. Babel, Y. Zhu, K.F. Cheng, W.C. Chen, S.A. Jenekhe, Adv. Funct. Mater. 17 (2007) 2542–2549.
[14] Y. Huang, Z. Wang, Z. Chen, Q. Zhang, Angew. Chem. Int. Ed. 58 (2019) 9696–9711.
[15] H. Wu, Y. Sun, L. Sun, et al., Chin. Chem. Lett. 32 (2021) 3007–3010.
[16] L. Gao, G.V. Baryshnikov, A. Ali, et al., Angew. Chem. Int. Ed. 63 (2024) e202318497.
[17] M.A. Niyas, S. Garain, K. Shoyama, F. Wurthner, Angew. Chem. Int. Ed. 63 (2024) e202406353.
[18] A.A. Kongasseri, S. Garain, S.N. Ansari, et al., Chem. Mater. 35 (2023) 7781–7788.
[19] B. Pigulski, K. Shoyama, M.J. Sun, F. Wurthner, J. Am. Chem. Soc. 144 (2022) 5718–5722.
[20] Y. Huang, J. Xing, Q. Gong, et al., Nat. Commun. 10 (2019) 169.
[21] H. Ye, G. Liu, S. Liu, et al., Angew. Chem. Int. Ed. 57 (2018) 1928–1932.
[22] A.S. Tayi, A.K. Shveyd, A.C. Sue, et al., Nature 488 (2012) 485–489.
[23] F. Kagawa, S. Horiuchi, H. Matsui, et al., Phys. Rev. Lett. 104 (2010) 227602.
[24] Y. Tokura, S. Koshihara, Y. Iwasa, et al., Phys. Rev. Lett. 63 (1989) 2405–2408.
[25] W. Zhu, L. Zhu, Y. Zou, et al., Adv. Mater. 28 (2016) 5954–5962.
[26] W. Zhu, R. Zheng, Y. Zhen, et al., J. Am. Chem. Soc. 137 (2015) 11038–11046.
[27] W. Zhu, R. Zheng, X. Fu, et al., Angew. Chem. Int. Ed. 54 (2015) 6785–6789.
[28] W. Zhu, L. Zhu, L. Sun, et al., Angew. Chem. Int. Ed. 55 (2016) 14023–14027.
[29] K. Wang, Z. Gao, W. Zhang, et al., Sci. Adv. 5 (2019) eaaw2953.
[30] Z. Wang, F. Yu, W. Chen, et al., Angew. Chem. Int. Ed. 59 (2020) 17580–17586.
[31] Y. Wang, G. Zhang, W. Zhang, et al., Small 12 (2016) 6554–6561.
[32] P. Yu, Y. Li, H. Zhao, et al., Small 17 (2021) e2006574.
[33] J. Guo, Y. Zeng, Y. Zhen, et al., Angew. Chem. Int. Ed. 61 (2022) e202202336.
[34] Y. Qin, J. Zhang, X. Zheng, et al., Adv. Mater. 26 (2014) 4093–4099.
[35] J. Zhang, H. Geng, T.S. Virk, et al., Adv. Mater. 24 (2012) 2603–2607.
[36] N.A. Mir, R. Dubey, G.R. Desiraju, Acc. Chem. Res. 52 (2019) 2210–2220.
[37] A. Vriza, A.B. Canaj, R. Vismara, et al., Chem. Sci. 12 (2020) 1702–1719.
[38] Y. Yoshida, Y. Kumagai, M. Mizuno, et al., Cryst. Growth Des. 15 (2015) 5513–5518.
[39] A.D. Bandrauk, K.D. Truong, C. Carlone, Can. J. Chem. 60 (1982) 588–595.
[40] X. Han, Y. Lei, Q. Liao, H. Fu, Angew. Chem. Int. Ed. 60 (2021) 3037–3046.
[41] Y. Wang, H. Wu, W. Zhu, et al., Angew. Chem. Int. Ed. 60 (2021) 6344–6350.
[42] H.T. Black, D.F. Perepichka, Angew. Chem. Int. Ed. 53 (2014) 2138–2142.
[43] M. Paul, G.R. Desiraju, Angew. Chem. Int. Ed. 58 (2019) 12027–12031.
[44] M.P. Zhuo, J.J. Wu, X.D. Wang, et al., Nat. Commun. 10 (2019) 3839.
[45] C.F. Xu, Y. Yu, Q. Lv, et al., Chin. Chem. Lett. 33 (2022) 3255–3258.
[46] M.D. Ward, W.S. Tang, L. Zhu, et al., Macromolecules 52 (2019) 7557–7563.
[47] Y. Sun, Y. Lei, W. Hu, W.Y. Wong, J. Am. Chem. Soc. 142 (2020) 7265–7269.
[48] S.P. Yelgaonkar, G. Campillo-Alvarado, L.R. MacGillivray, J. Am. Chem. Soc. 142 (2020) 20772–20777.
[49] J. Zhang, W. Xu, P. Sheng, G. Zhao, D. Zhu, Acc. Chem. Res. 50 (2017) 1654–1662.
[50] L. Sun, W. Zhu, X. Zhang, et al., J. Am. Chem. Soc. 143 (2021) 19243–19256.
[51] Y. Takahashi, T. Hasegawa, Y. Abe, Y. Tokura, G. Saito, Appl. Phys. Lett. 88 (2006) 073504.
[52] M. Sakai, H. Sakuma, Y. Ito, et al., Phys. Rev. B 76 (2007) 045111.
[53] W. Zhu, Y. Yi, Y. Zhen, W. Hu, Small 11 (2015) 2150–2156.
[54] M. Jiang, S. Li, C. Zhen, et al., Front. Optoelectron. 15 (2022) 21.
[55] S.K. Park, S. Varghese, J.H. Kim, et al., J. Am. Chem. Soc. 135 (2013) 4757–4764.
[56] S.K. Park, J.H. Kim, T. Ohto, et al., Adv. Mater. 29 (2017) 1701346.
[57] J. Liu, H. Zhang, H. Dong, et al., Nat. Commun. 6 (2015) 10032.
[58] H. Geng, L. Zhu, Y. Yi, D. Zhu, Z. Shuai, Chem. Mater. 31 (2019) 6424–6434.
[59] G. Zhao, H. Dong, Q. Liao, et al., Nat. Commun. 9 (2018) 4790.
[60] H. Ju, K. Wang, J. Zhang, et al., Chem. Mater. 29 (2017) 3580–3588.